

Classification of CMEs Based on Their Dynamics

J. Nicewicz¹ · G. Michalek¹

Received: 4 December 2015 / Accepted: 4 May 2016 / Published online: 26 May 2016
© The Author(s) 2016. This article is published with open access at Springerlink.com

Abstract A large set of coronal mass ejections CMEs (6621) has been selected to study their dynamics seen with the *Large Angle and Spectroscopic Coronagraph* (LASCO) onboard the *Solar and Heliospheric Observatory* (SOHO) field of view (LFOV). These events were selected based on having at least six height-time measurements so that their dynamic properties, in the LFOV, can be evaluated with reasonable accuracy. Height-time measurements (in the SOHO/LASCO catalog) were used to determine the velocities and accelerations of individual CMEs at successive distances from the Sun. Linear and quadratic functions were fitted to these data points. On the basis of the best fits to the velocity data points, we were able to classify CMEs into four groups. The types of CMEs do not only have different dynamic behaviors but also different masses, widths, velocities, and accelerations. We also show that these groups of events are initiated by different onset mechanisms. The results of our study allow us to present a consistent classification of CMEs based on their dynamics.

Keywords Sun · Solar activity · Coronal mass ejections

1. Introduction

Coronal mass ejections (CMEs) are large expulsions of magnetized plasma from the Sun. They show a remarkably rich variety of morphological and kinematical characteristics (Yashiro *et al.*, 2004). After their discovery in the early 1970s, they were studied intensively during the P78-1 satellite mission. The structure of CMEs was analyzed by Howard *et al.* (1985) and arranged into nine structural classes: spike, double spike, multiple spike, curved front, loop, halo, complex, streamer blowout, and diffuse fan. This study has also shown that the properties of CMEs depend strongly on their shapes. The coronagraphs of the *Large Angle and Spectroscopic Coronagraph* (LASCO) onboard the *Solar and Heliospheric Observatory* (SOHO) have been extensively observing the solar corona since 1996 and have recorded thousands of CMEs (Brueckner *et al.*, 1995). Images from SOHO/LASCO have

✉ G. Michalek
michalek@oa.uj.edu.pl

¹ Astronomical Observatory of Jagiellonian University, Cracow, Poland

revealed that ejections can take various shapes, which are difficult to categorize using a simple structural classification. Some of the properties of the SOHO/LASCO CMEs have been described using a variety of properties (e.g., Howard *et al.*, 1997; St. Cyr *et al.*, 2000; Gopalswamy *et al.*, 2003; Gopalswamy *et al.*, 2004; Yashiro *et al.*, 2003) such as intensity, angular span width, and speed. Dai, Zong, and Tang (2002) simplified Howard's classification and arranged CMEs into three intensity categories: strong (including halo and complex), middle (including double spike, multiple spike, and loops), and weak (including spike, streamer blowout, and diffuse fan). This categorization was used to build an automatic algorithm to detect and classify CMEs (Ming *et al.*, 2006). The algorithm was mainly used to distinguish strong CMEs, which are likely to be geoeffective, from weak CMEs. Despite the fact that CMEs are the most energetic and most important phenomena for space weather forecast, a unique coherent and widely accepted method of CME classification has not been developed.

Recently, Michalek (2012) has developed a new technique to analyze the dynamics of CMEs. Based on their acceleration behavior, he was able to classify the observed events into four different types. It was also demonstrated that the acceleration may change significantly during a CME propagation in the LASCO field of view (LFOV). To carry out a more accurate investigation of the dynamics of CMEs it is important to evaluate the acceleration values at different distances from the Sun.

In the present study, we consider a set of CMEs recorded by LASCO during 1996–2004, having at least six height-time data points in SOHO/LASCO CME catalog.¹ The aim of the present article is to study the evolution of the velocity and acceleration of CMEs as a function of distance from the Sun and attempt to classify them.

This article is organized as follows. In Section 2, the data and method used for this study are described. Results of our analysis are discussed in Section 3. The initiation of different types of events is described in Section 4. In Section 5, we present a classification of CMEs. Finally, our discussion and conclusions are presented in Section 6.

2. Method to Analyze the Dynamics of CMEs

In this section we describe the method and data selection used to classify the CMEs.

2.1. Data Selection

For this study we employed CMEs detected by the LASCO coronagraphs from January 1996 to December 2004 and included in the SOHO/LASCO CME catalog (Yashiro *et al.*, 2004). Out of the 9309 CMEs recorded during this period of time, we chose 6621 CMEs. These selected events have at least six height-time measurements. The propagation of CMEs is traced manually by measuring the plane-of-sky heliocentric distance [r] of the leading edges. The error in these measurements could be large and dependent on the sharpness of the leading edge of a particular event. In many studies, however, the influence of measurement errors on the estimated quantities is neglected. Wen, Maia, and Wang (2007), using data from the SOHO/LASCO CME catalog, estimated the measurement errors as a function of the distance from the Sun. They have shown that the error in the leading-edge position of CMEs grows with the square of the distance in the C2 LFOV and with the square root of the distance in the C3 LFOV. These random errors significantly affect the determination of a CME

¹http://cdaw.gsfc.nasa.gov/CME_list/.

velocity and acceleration. To carry out a more accurate investigation of the dynamics of CMEs, in this study a statistical analysis of a large population of CMEs having at least six height-time measurements is performed. Using our data selection, we can estimate the acceleration and velocity of CMEs with good accuracy and we can also examine the evolution of these parameters with the distance from the Sun. Since we have selected events with at least six height-time points, our sample is biased to CMEs with velocities up to 1500 km s^{-1} . The fastest CMEs ($V > 1500 \text{ km s}^{-1}$) are excluded but these events are very rare and their exclusion does not significantly affect our results.

2.2. Method to Classify CMEs

To study the dynamics of CMEs we consider the evolution of their velocities and accelerations with the distance from the solar surface. Therefore, from two successive data points, we determine the velocities:

$$v_{(t_{i+1}-t_i)/2} = \frac{r_{i+1} - r_i}{t_{i+1} - t_i}. \quad (1)$$

Next, from two successive velocity data points the acceleration is evaluated as

$$a_{(t_{i+1}-t_i)/2} = \frac{v_{i+1} - v_i}{t_{i+1} - t_i}. \quad (2)$$

Velocities and accelerations evaluated in this way are used in our further analysis. Linear and quadratic functions were fitted to the velocity-time and acceleration-time profiles for all the considered CMEs. Then, comparing the errors obtained using the least-square method, a better fit for each CME was selected. This procedure was applied for both velocity and acceleration data points. The better fit gives variations of velocity and acceleration for each CME. According to their velocity behavior we distinguish four types of CMEs: continuously accelerated (AA, fitted by a straight line with a positive slope), continuously decelerated (DD, fitted by a linear function with a negative slope), accelerated and next decelerated (AD, fitted by a parabola with a downward curvature), and decelerated and next accelerated (DA, fitted by a parabola with an upward curvature). A similar distinction can be made for the acceleration. In this case we can also distinguish four classes of events: continuously increasing acceleration (II, fitted by a straight line with a positive slope), continuously falling acceleration (FF, fitted by a linear function with a negative slope), increasing and next falling acceleration (IF, fitted by a parabola with a downward curvature) and falling and next increasing acceleration (FI, fitted by a parabola with an upward curvature). We carried out this analysis for all the events in our sample and we sorted them using these selection criteria. In this study we used height-time points determined manually. These measurements are subject to uncertainties. To obtain reasonable parabolic and almost linear fits to our speed- and acceleration-time profiles, only CMEs having at least six height-time measurements were selected. This arbitrary selection criterion ensures that the parabola and almost straight line are fitted at least to five and four points, respectively.

3. Characteristic of Different Types of CMEs

The classification of CMEs, based on their dynamic properties, can be formally applied to categorize of ejections. However, it is interesting to know whether this division applies also to other observational parameters (OPs) of CMEs. We carried out a statistical study of key CME parameters (acceleration, angular width, velocity, mass) for the different types of CMEs.

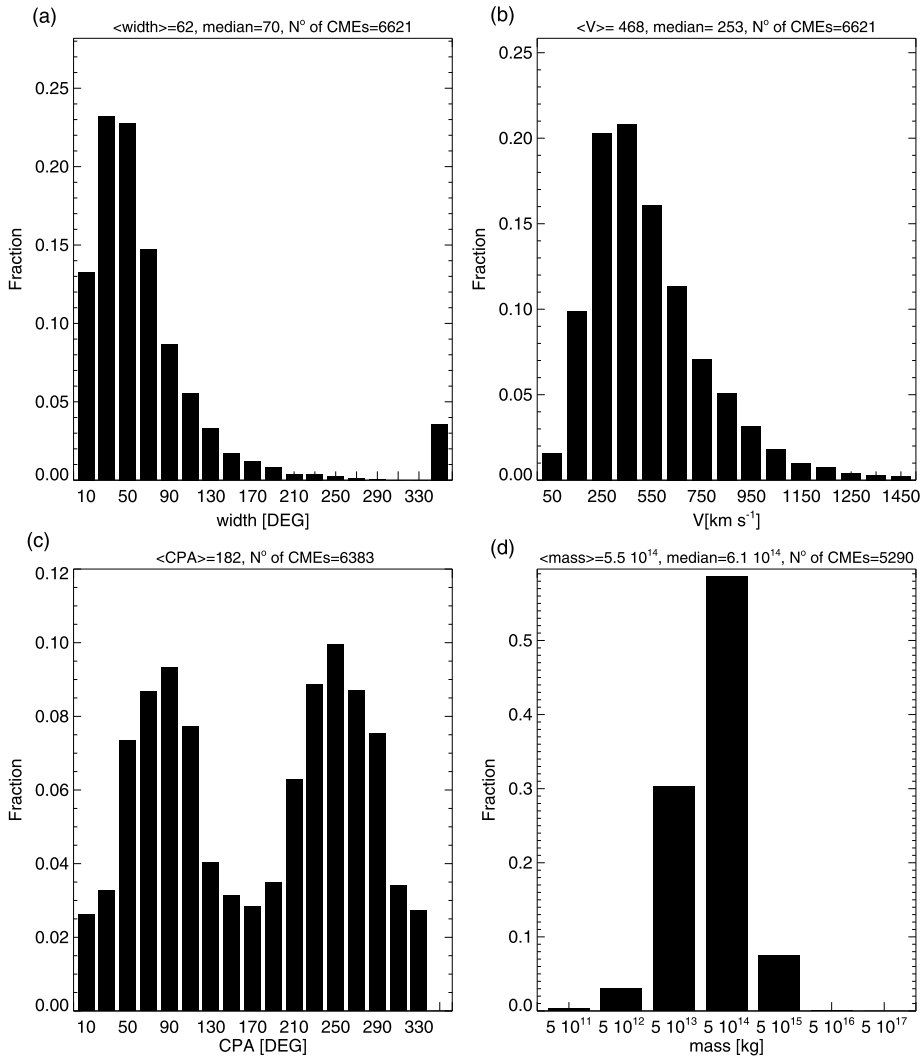


Figure 1 Statistical properties of all the considered CMEs. Panels a–d display distributions of width, velocity, central position angle (CPA), and mass. At the top of the panels average and median values for each parameter are displayed.

3.1. Statistical Characteristics of CMEs Divided Based on Their Speed Variations

The statistical characteristics of CMEs divided based on their speed variation are shown in 12 successive figures (Figures 3–14). For comparison, in Figures 1 and 2 properties of all the considered CMEs are presented. The same analysis of the OPs has been done for the different classes of events so it is worth, at this point, to explain in detail what is displayed in each panel of Figures 1 and 2. Figures 1a–d display the distributions of width, velocity, central position angle, and mass. Figures 2a–c show the scatter plots between the acceleration and other parameters characterizing CMEs. The next three panels, d–f, present the more detailed relationship between the acceleration and the CME width, mass, and velocity.

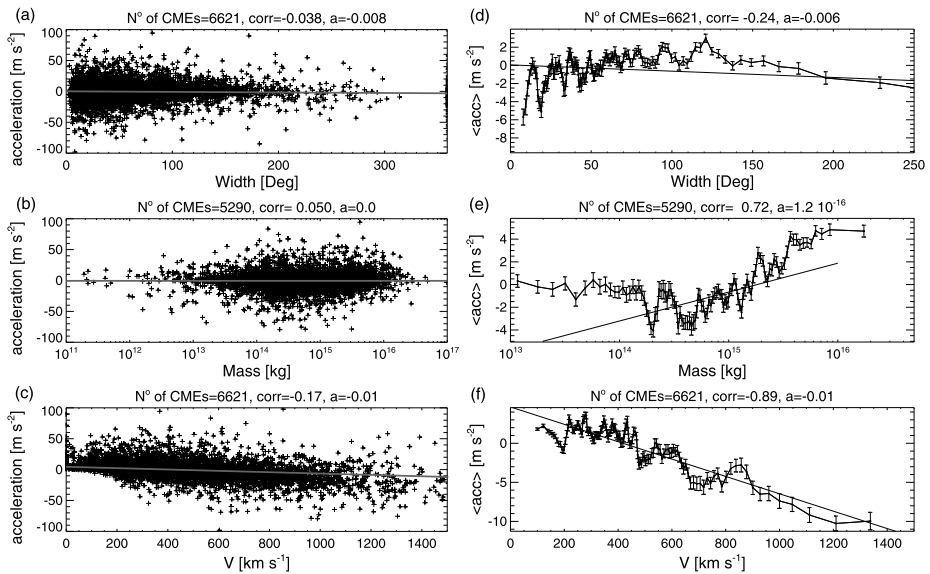


Figure 2 Statistical properties of all the considered CMEs. (a)–(c) show scatter plots between the accelerations (from the SOHO/LASCO catalog) and widths, masses, and velocities. (d)–(f) show the relationship between the accelerations (calculated as discussed in the text) and the CME widths, masses, and velocities. Solid lines (panels a–f) are linear fits to the data points. Error bars (panels d–f) were obtained from the dispersion determined for the sub-sample of 200 successive CMEs. At the top of the panels correlation coefficients and slopes of linear fits to the data points are shown.

To create the latter panels, we separated CMEs in sub-samples with successively increasing values of average widths, masses and speeds. For this purpose, we ordered our CME sample by their width, mass, and speed. Next, we created smaller sub-samples consisting of 200 successive CMEs, where each next sub-sample was shifted by 50 events toward higher widths, masses, and velocities, respectively. In this way we obtained a large number of partly overlapping sub-samples ordered by successively increasing mean widths, masses, and speeds. For each sub-sample, the average value of a parameter was calculated and then used to create the graphs. The same procedure was followed to create the respective graphs in Figures 3–10.

For all the considered CMEs (Figure 1) the average values of the OPs are very similar to those obtained by other authors considering statistical characteristics of CMEs included in the SOHO/LASCO catalog (e.g., Yashiro *et al.*, 2004). Our study shows a negative correlation between the acceleration and speed (panels c and f in Figure 2). It is worth to note that in panel (f) we can observe a transition from positive to negative acceleration. The point when the acceleration is zero can be interpreted as the average solar wind speed, which according to our method is about 410 km s⁻¹. Interesting results are displayed in panels d and e. Panel d indicates that the narrowest (width < 60°) and the widest (width > 200°) CMEs are mostly decelerated while those with intermediate widths are accelerated. A different trend is observed for masses. The less massive CMEs are mostly decelerated (mass < 5 × 10¹⁴ kg) while the more massive ones are accelerated.

In Figures 3 and 4 we show the statistical characteristics of the AA CMEs. This is the most numerous group of CMEs (32 % of the total number we analyzed). On average, they have similar widths ($\langle \text{width} \rangle = 61^\circ$) and masses ($\langle \text{mass} \rangle = 5.4 \times 10^{14}$ kg) as all

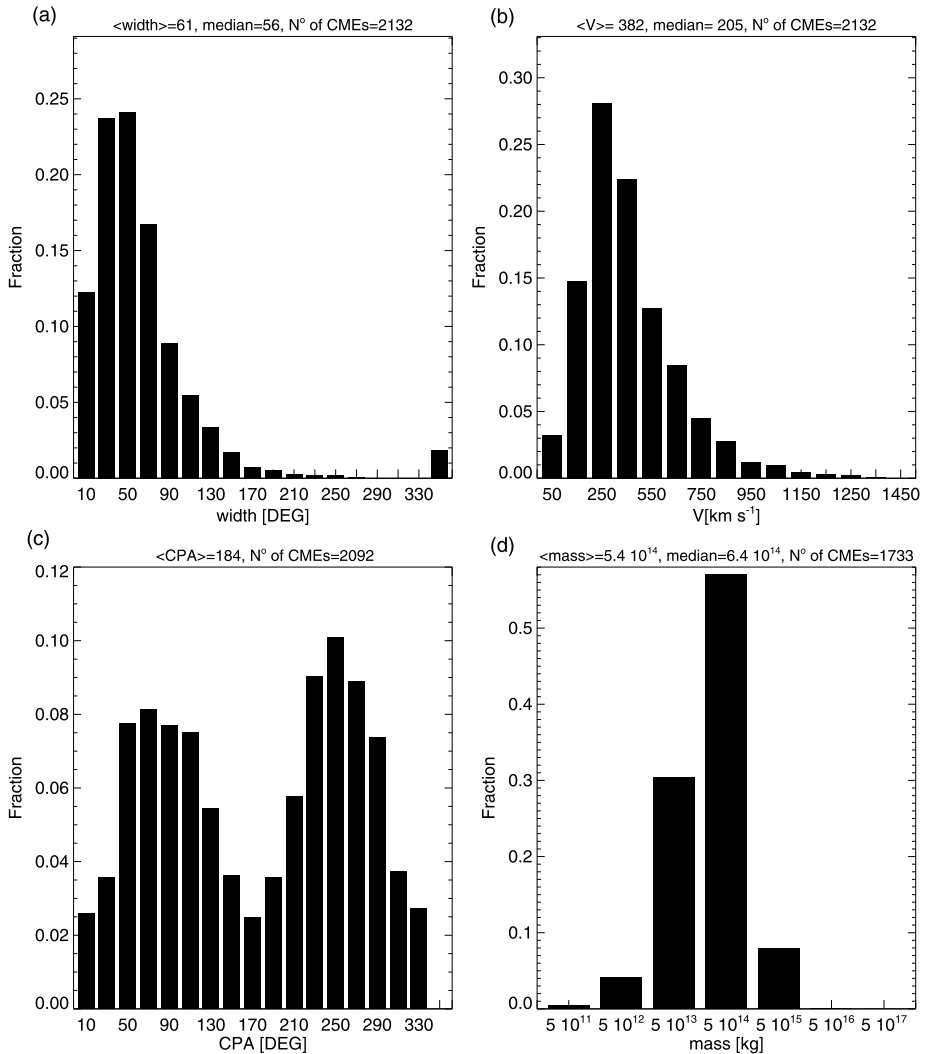


Figure 3 Statistical properties of the AA CMEs. (a)–(d) display distributions of width, velocity, central position angle (CPA), and mass. At the top of the panels average and median values for each parameter are displayed.

the considered CMEs. However, some of their properties differ significantly from the other types of CMEs. They are, on average, the slowest events in the whole population of CMEs ($\langle \text{velocity} \rangle = 382 \text{ km s}^{-1}$). They show a significant positive correlation between acceleration and speed (the correlation coefficient is 0.97; see Figure 4f. Figures 4d–e show that the acceleration of the AA CMEs significantly decreases with their width and mass. The narrowest and least massive events have the largest positive accelerations. In the LFOV the dynamics of these events is dominated by the propelling force. More massive and wider CMEs have lower positive acceleration due to larger inertia and drag force.

In Figures 5 and 6 the statistical characteristics of the DD type of CMEs is presented. This is the second most numerous group of CMEs (27 % of the total number we analyzed).

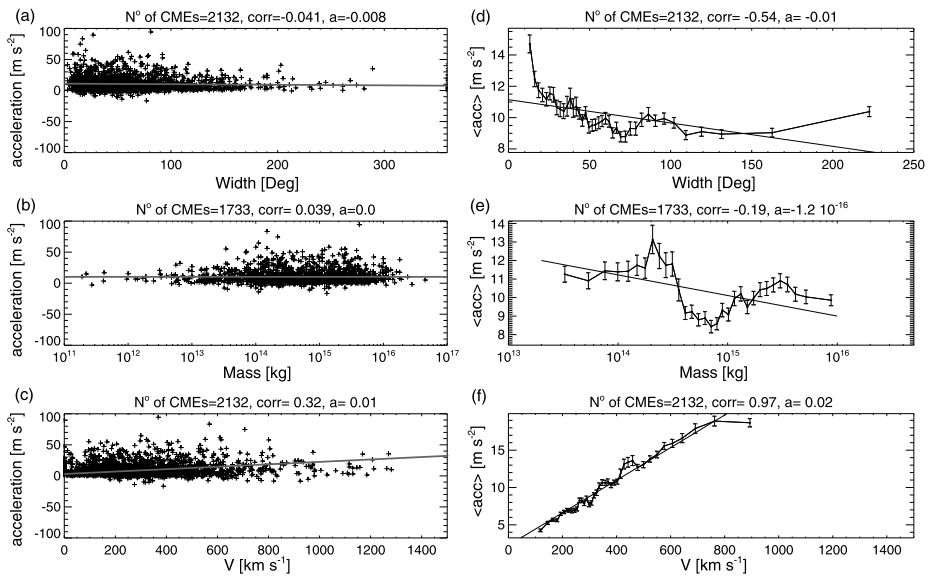


Figure 4 Statistical properties of the AA CMEs. (a)–(c) show scatter plots between the accelerations (from the SOHO/LASCO catalog) and widths, masses, and velocities. (d)–(f) show the relationship between the accelerations (calculated as discussed in the text) and the CME widths, masses, and velocities. Solid lines (panels a–f) are linear fits to the data points. Error bars (panels d–f) were obtained from the dispersion determined for the sub-sample of 200 successive CMEs. At the top of the panels correlation coefficients and slopes of linear fits to the data point are shown.

On average, they have similar widths ($\langle \text{width} \rangle = 58^\circ$) as all the considered CMEs. They are the least massive events ($\langle \text{mass} \rangle = 4.3 \times 10^{14}$ kg) in comparison to the other types of events. The DD CMEs are fast ($\langle \text{velocity} \rangle = 501$ km s⁻¹) and present a significant negative correlation coefficient between acceleration and speed (the correlation coefficient is -0.42 in Figure 6c and -0.98 in Figure 6f). Interesting results are presented in the panels d and e. The narrowest and widest events have the most significant negative accelerations of up to -18 km s⁻¹. Inspecting the panel e, we see that the deceleration of these CMEs decreases with their mass. This means that after the very effective and short acceleration, the dynamics of these events is dominated by their inertia.

In Figures 7 and 8 the statistical characteristics of the AD CMEs is shown. About 20 % of all the CMEs belong to this type. On average, they are the widest ($\langle \text{width} \rangle = 67^\circ$), the most massive (mass = 7.1×10^{14} kg) and very close to the fastest ($\langle \text{velocity} \rangle = 512$ km s⁻¹) ejections. The AD CMEs show a positive correlation between acceleration and speed (the correlation coefficient is 0.85; see Figure 8f). Narrower (width < 70°) and less massive (mass ≤ 1.0×10^{15} kg) events have constant velocities. Wider and more massive events show a positive acceleration (up to 8.0 m s⁻²).

In Figures 9 and 10 the statistical characteristics of the DA CMEs is shown. About 20 % of all the CMEs belong to this type. On average, they are wide ($\langle \text{width} \rangle = 66^\circ$), massive ($\langle \text{mass} \rangle = 6.3 \times 10^{14}$ kg) and the fastest ($\langle \text{velocity} \rangle = 516$ km s⁻¹) ejections. These events show a significant negative correlation between the acceleration and speed (the correlation coefficient is -0.98 ; see Figure 10f). The narrowest (width < 30°) and widest (width > 180°) have, on average, the most significant deceleration (up to -5.0 m s⁻²).

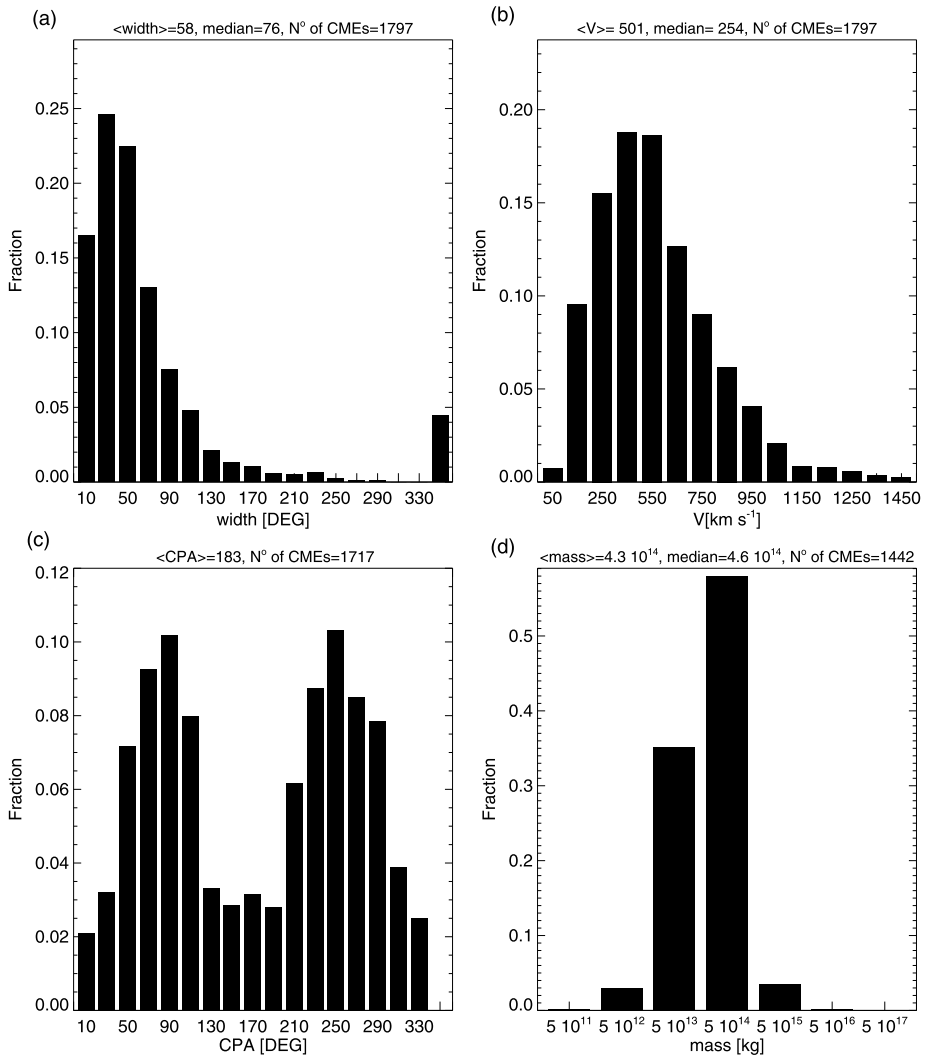


Figure 5 Statistical properties of the DD CMEs. (a)–(d) display distributions of width, velocity, central position angle (CPA), and mass. At the top of the panels average and median values for each parameter are displayed.

In Figure 11 the distributions of the acceleration for all the types of CMEs are displayed. If we consider all the events (distribution not shown in Figure 11), on average they are not accelerated ($\langle \text{acceleration} \rangle = -0.56 \text{ m s}^{-2}$). However, the different types of CMEs show clear trends when we consider their accelerations. The AA type of CMEs have the most significant positive acceleration on average ($\langle \text{acceleration} \rangle = 10.4 \text{ m s}^{-2}$). The AD type of CMEs show a similar tendency, though it is not so clear ($\langle \text{acceleration} \rangle = 1.6 \text{ m s}^{-2}$). The strongest deceleration is shown by the DD type of CMEs ($\langle \text{acceleration} \rangle = -13.7 \text{ m s}^{-2}$). This trend is also clearly observed in the case of the DA type of CMEs ($\langle \text{acceleration} \rangle = -3.08 \text{ m s}^{-2}$).

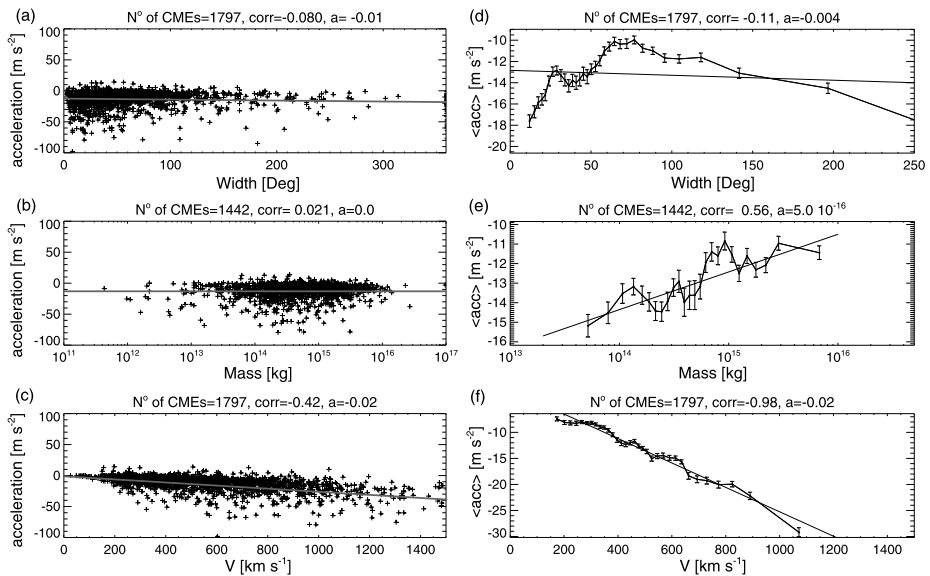


Figure 6 Statistical properties of the DD CMEs. (a)–(c) show scatter plots between the accelerations (from the SOHO/LASCO catalog) and widths, masses, and velocities. (d)–(f) show the relationship between the accelerations (calculated as discussed in the text) and the CME widths, masses, and velocities. Solid lines (panels a–f) are linear fits to the data points. Error bars (panels d–f) were obtained from the dispersion determined for the sub-sample of 200 successive CMEs. At the top of the panels correlation coefficients and slopes of linear fits to the data point are shown.

To have a more complete description of the different types of CMEs, we study the relation between the CME rate and the solar cycle. The CME rate (total number of each type of events *per* year and percentage of each type of events *per* year) for the different categories of CMEs are displayed in Figures 12 and 13. The considered classes of CMEs appear during the whole solar activity cycle. However, the AA and AD are more likely to appear during the minimum phase of the solar activity cycle. In the period of time 1996–1998, 70 % of all the CMEs belong to these two classes of events. The other two classes, AD and DD, are mostly launched during the maximum phase of the solar activity cycle. One thing that is interesting in Figures 12 and 13 is an increase (of about 20 % in comparison with the occurrence rates in 2000 and 2002) in the occurrence rate of the AA CMEs, which was observed in 2001 and a decrease in the occurrence rate of the DD CMEs.

The same statistical analysis was carried out for CMEs divided based on their acceleration variations. However, this way of dividing the events did not produce any clear result.

4. Initiation of the Different Types of CMEs

In the previous sections we have defined four distinctly different types of CMEs. These types of events differ in their dynamic and kinematic behavior observed in the LFOV. Therefore, there must be a physical reason that determines these different behaviors. Michalek (2009) studied the relationship between flares and CMEs. To find a temporal association between flares and CMEs, it was necessary to determine the onset time of CMEs at the Sun. To do so Michalek (2009) employed linear or quadratic (depending on which one

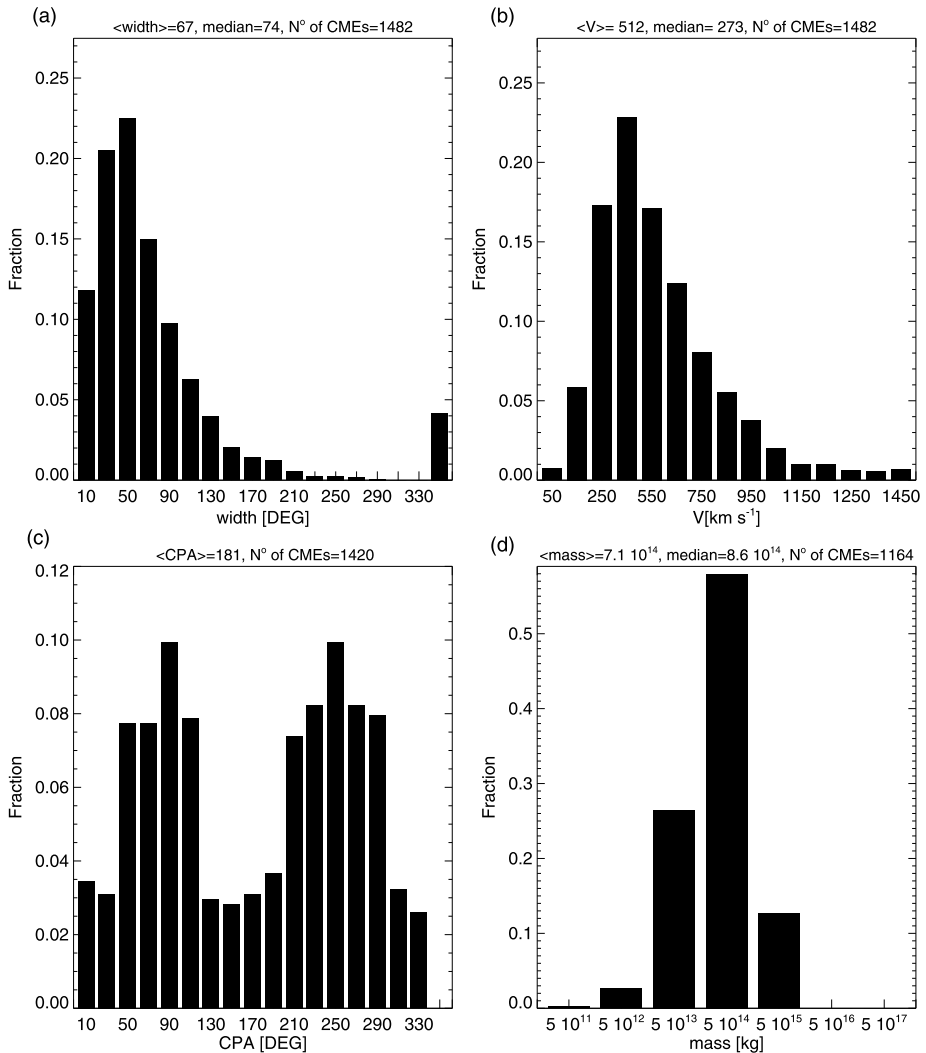


Figure 7 Statistical properties of the AD CMEs. (a)–(d) display distributions of width, velocity, central position angle (CPA), and mass. At the top of the panels average and median values for each parameter are displayed.

was better) fits to the height-time plots. Next, the onset times of CMEs were compared to the onset times of the associated X-flares. He considered two types of flare-associated CMEs: CMEs that follow or precede the flare onset time. It was demonstrated that both samples have quite different characteristics. CMEs appearing after flares (AF) tend to be decelerated (median acceleration = -5.0 m s^{-2}), fast (median velocity = 519 km s^{-1}), and physically related to flares. Events ejected before flares (BF) were mostly accelerated (median acceleration = 5.4 m s^{-2}) and slower (median velocity = 487 km s^{-1}). The characteristics of these two groups of CMEs are similar to those of the CME types introduced in the present work. The AA and AD CMEs are similar to the BF events, while the DA and DD CMEs look like the AF ejections.

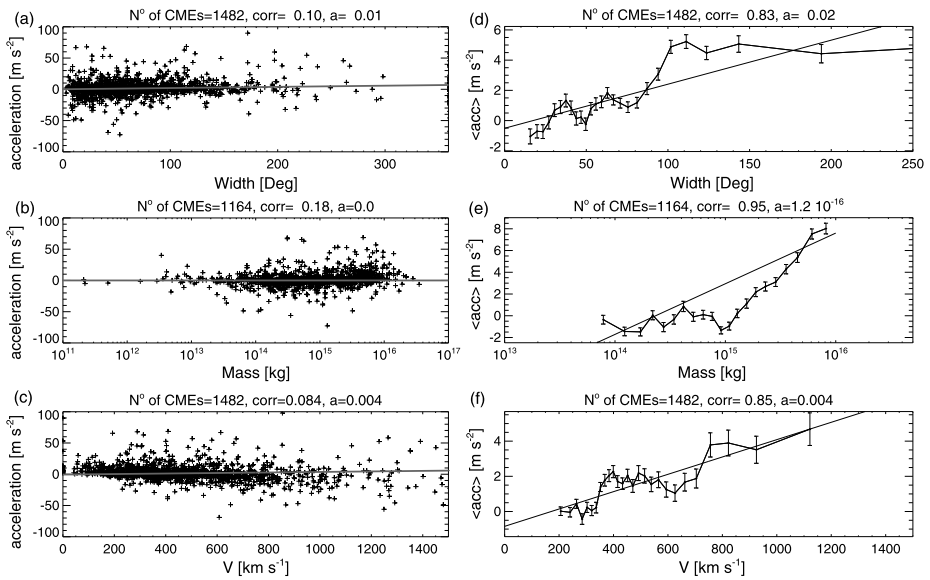


Figure 8 Statistical properties of the AD CMEs. (a)–(c) show scatter plots between the accelerations (from the SOHO/LASCO catalog) and widths, masses, and velocities. (d)–(f) show the relationship between the accelerations (calculated as discussed in the text) and the CME widths, masses, and velocities. Solid lines (panels a–f) are linear fits to the data points. Error bars (panels d–f) were obtained from the dispersion determined for the sub-sample of 200 successive CMEs. At the top of the panels correlation coefficients and slopes of linear fits to the data point are shown.

In Figure 14 the distributions of the four types of events for the BF and AF CMEs are shown. To obtain this figure we have used the sub-sample of flare-associated CMEs studied by Michalek (2009). It is clearly seen that the AA CMEs tend to be launched before flares (~40 % belong to this category CMEs), while the DD CMEs are likely to be ejected after flares (~40 % belong to this category). The other two types of CMEs (AD and DA) do not show any systematic temporal relation with the associated flares. Almost as many of them appear before the associated flares as after them. The AA CMEs appear on average eight minutes before the onset of the associated flares. The DD CMEs are launched on average 19 minutes after the associated flares. The AD and DA CMEs appear almost simultaneously with the associated flares.

5. Classification of CMEs

In Section 3, we discussed a classification of CMEs based mainly on their kinetic properties, which we associated to other observational parameters. In Section 4, we combined our classification with the results of Michalek (2009) and related our CME types to the onset time of the associated flares. Table 1 summarizes our results. The successive rows of the table show the classes of CMEs, the percentage of occurrence, and the general characteristics of the four key OPs describing CMEs (width, mass, speed, and acceleration). Next, the relation between the acceleration and speed is shown. The following row indicates the phase of the solar activity cycle when the different types of ejections have the highest probability of occurrence. The last two rows show the relation to the associated flares.

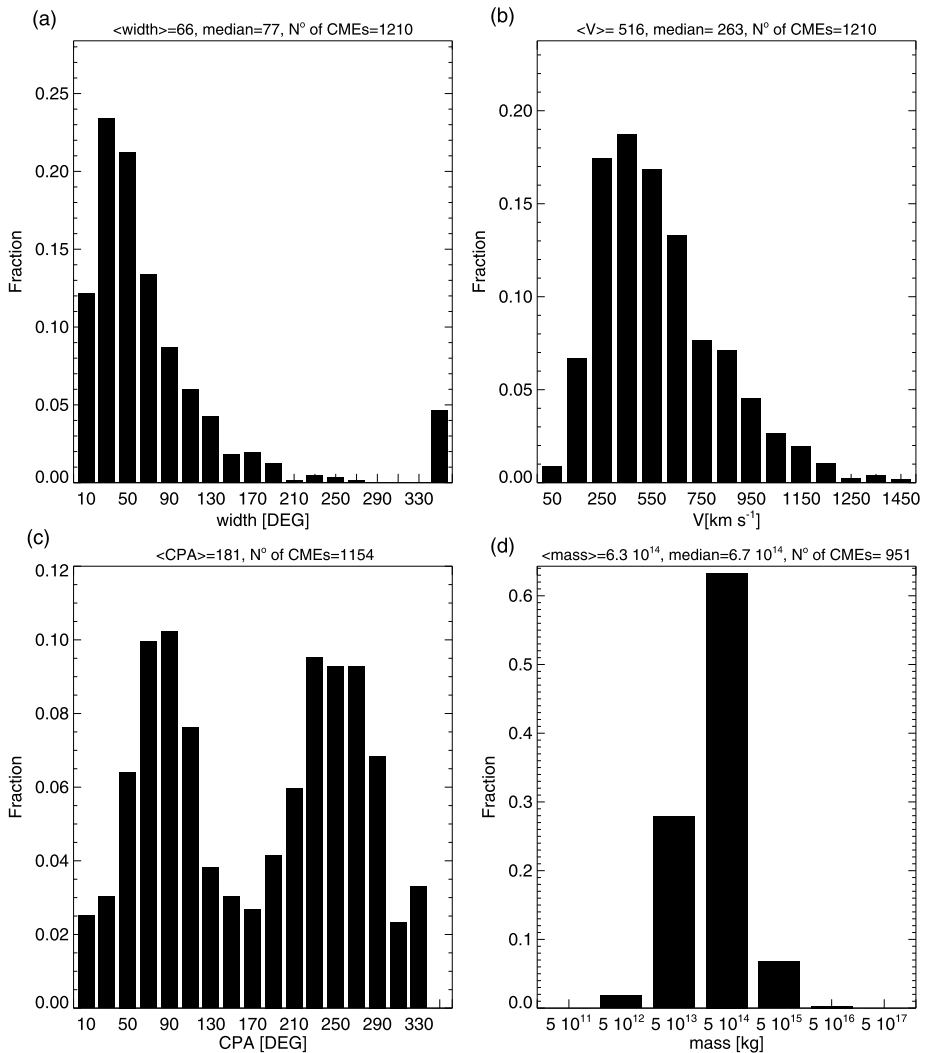


Figure 9 Statistical properties of the DA CMEs. (a)–(d) display distributions of width, velocity, central position angle (CPA), and mass. At the top of the panels average and median values for each parameter are displayed.

6. Summary and Discussion

We studied a subset of 6621 CMEs during the period of 1996–2004 for which six height-time measurements were available in SOHO/LASCO CME catalog. This method of selection excludes from the study the fastest events ($V > 1500 \text{ km s}^{-1}$). On the other hand, it allows us to accurately analyze the dynamics of CMEs in the LFOV.

Height-time measurements were used to determine the velocities and accelerations of individual CMEs. Then quadratic and linear functions were fitted to these speed- and acceleration-time profiles. On the basis of the best fit to the velocity data points, we were able to classify CMEs into four types (AA, AD, DA, and DD classes). The types of CMEs do

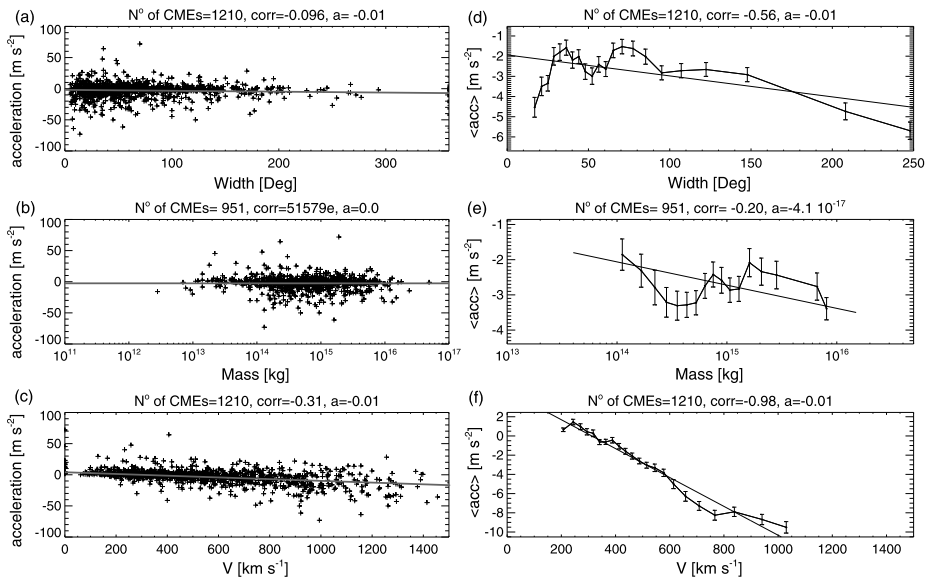


Figure 10 Statistical properties of the DA CMEs. (a)–(c) show scatter plots between the accelerations (from the SOHO/LASCO catalog) and widths, masses, and velocities. (d)–(f) show the relationship between the accelerations (calculated as discussed in the text) and the CME widths, masses, and velocities. Solid lines (panels a–f) are linear fits to the data points. Error bars (panels d–f) were obtained from the dispersion determined for the sub-sample of 200 successive CMEs. At the top of the panels correlation coefficients and slopes of linear fits to the data point are shown.

Table 1 Classification of CMEs. The abbreviation sig. in the second, fourth, and fifth columns means significantly.

Class	AA	AD	DA	DD
Percentage	≥ 30 %	~ 20 %	~ 20 %	~ 30 %
Width	typical	widest	wide	narrowest
Mass	typical	most massive	massive	least massive
Speed	slowest	fast	fastest	fast
Acceleration	sig. positive	positive	negative	sig. negative
Acceleration versus speed	sig. positive	positive	sig. negative	sig. negative
Preferred phase of solar cycle	minimum	minimum	maximum	maximum
Onset	before the flares	not clear	not clear	after the flares

not only have different dynamic behaviors, but also different masses, widths, velocities, and accelerations. The characteristics of the different types of CMEs are summarized in Table 1.

To explain the differences in the dynamic behaviors of the various types of ejections, we analyzed their temporal association with flares. This association could indicate which mechanism is responsible for the eruption (see Forbes, 2000, and references therein). AA CMEs are launched before the flares and could be explained by an ideal-resistive hybrid model (e.g., Lin *et al.*, 1998). An ejection in this scenario starts with an ideal MHD process

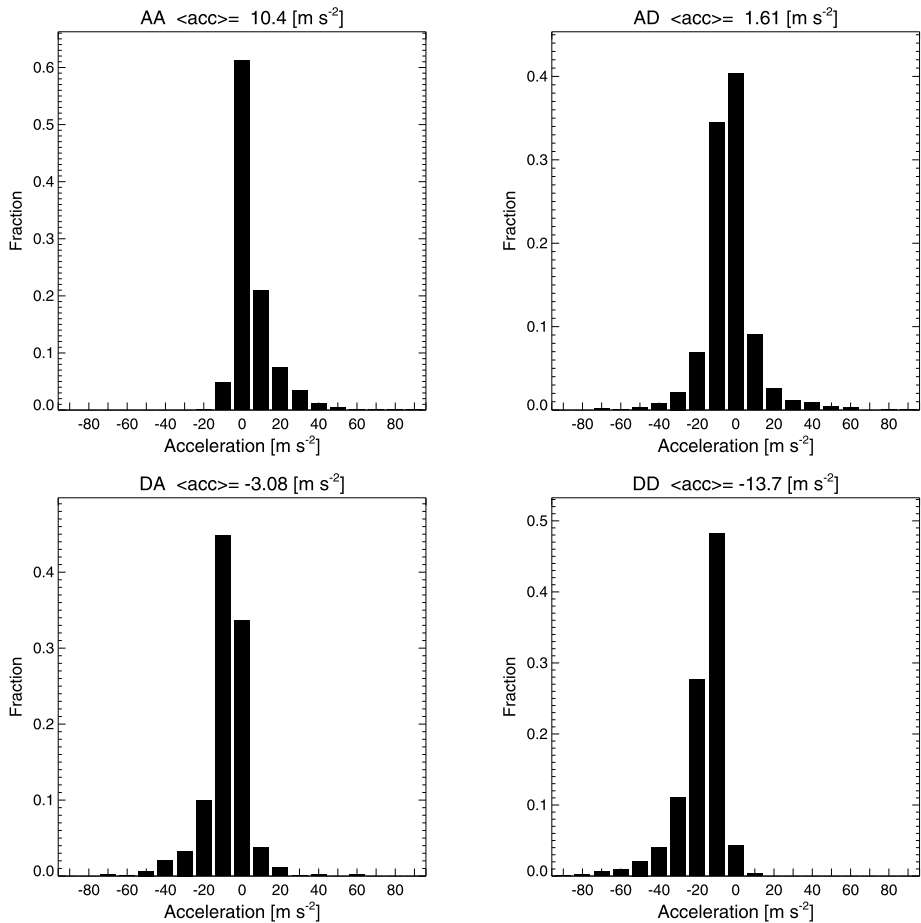


Figure 11 The distributions of the acceleration for all CME types. The successive panels correspond to the AA, AD, DA, and DD CME types.

that is further followed by resistive reconnection when the flare is triggered. This scenario can explain the low velocities and prolonged accelerations observed for these events in the LFOV. DD CMEs originate after the flare onset. This suggests that resistive magnetic reconnection should play the most important role during the initiation of these events (*e.g.*, Mikić and Linker, 1994; Antiochos, DeVore, and Klimchuk, 1999). The release of the free magnetic energy starts before the ejection of the CME. This scenario can explain the impulsive acceleration of these CMEs (close to the Sun) and their deceleration in the LFOV. For the two other types of CMEs (AD and DA) we are not able to recognize which of these processes is the most important. They are complex events and probably both scenarios are feasible. These CMEs should be more intensively studied in the future.

Images from the SOHO satellite have revealed that ejections can take various shapes which are difficult to characterize using a simple structural classification. We suggest that the consistent method of CME classification presented in this article is more general and could be developed to include other event features (*e.g.* the acceleration data points, the active region characteristics).

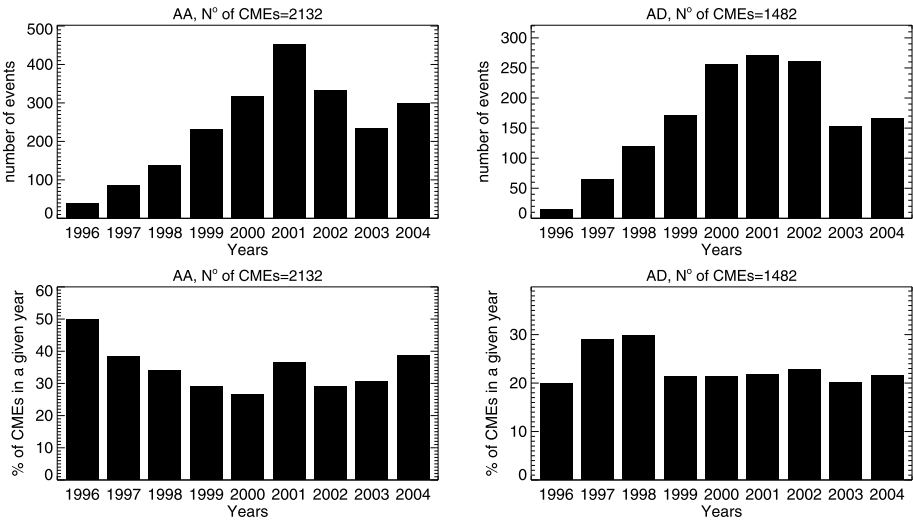


Figure 12 CME rate *versus* year for AA (left panels) and AD (right panels) classes. The upper panels show the total number of events *per* year. The lower panels show the percentage of events *per* year. The percentage of events *per* year was calculated dividing of the total number of each class by the total number of all the events in a given year.

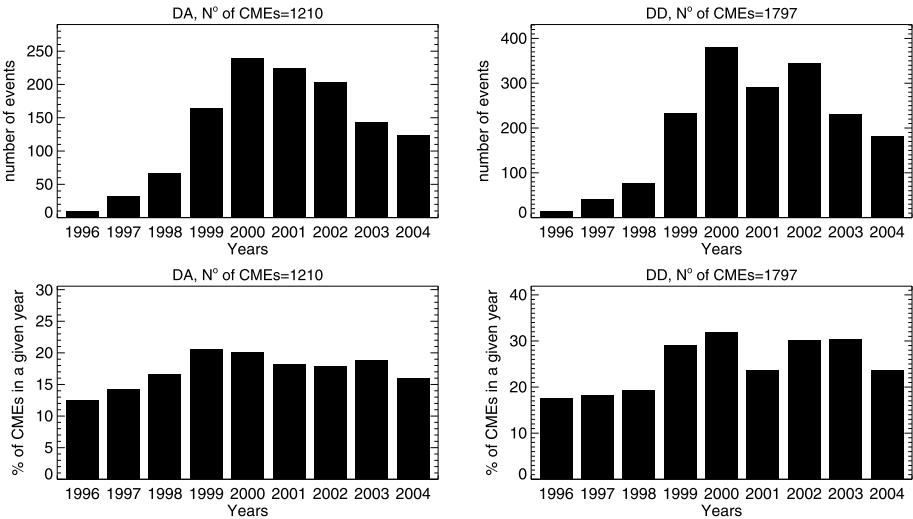
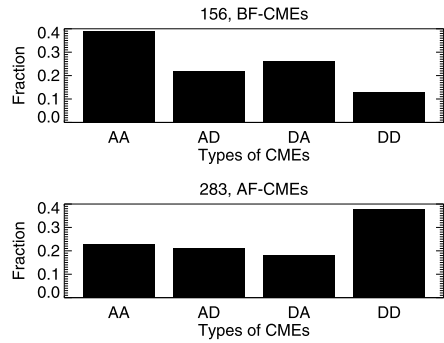


Figure 13 CME rate *versus* year for DA (left panels) and DD (right panels) classes. The upper panels show the total number of events *per* year. The lower panels show the percentage of events *per* year. The percentage of events *per* year was calculated dividing of the total number of each class by the total number of all the events in a given year.

The study of CME accelerations and velocities is very difficult due to the presence of significant and random measurement errors. Only statistical analysis of large samples of events, as the one carried out in this article, can provide reliable results.

Figure 14 The distributions of the four types of events for the BF (top panel) and AF CMEs (bottom panel).



Coronagraphic observations, recording photospheric photons scattered by electrons in the solar corona, do not allow us to unambiguously find many properties of CMEs in space. The basic characteristics of CMEs, such as velocity, acceleration, heliocentric distance, and width, are determined in the plane of the sky and are subject to projection effects. These effects mostly depend on the source location on the Sun and it is very difficult to estimate their influence on measured values. Because of projection effects, the apparent velocities and accelerations are lower and the apparent widths larger than the values in space. All relations between these parameters must be treated with caution.

Acknowledgements Grzegorz Michalek and Janusz Nicewicz were supported by NCN through the grant UMO-2013/09/B/ST9/00034. We are very grateful to the referee of this article for very important comments, which helped to improve it.

Disclosure of Potential Conflicts of Interest The authors declare that they have no conflicts of interest.

Open Access This article is distributed under the terms of the Creative Commons Attribution 4.0 International License (<http://creativecommons.org/licenses/by/4.0/>), which permits unrestricted use, distribution, and reproduction in any medium, provided you give appropriate credit to the original author(s) and the source, provide a link to the Creative Commons license, and indicate if changes were made.

References

- Antiochos, S.K., DeVore, C.R., Klimchuk, J.A.: 1999, *Astrophys. J.* **510**, 485. DOI.
- Brueckner, G.E., Howard, R.A., Koomen, M.J., Korendyke, C.M., Michels, D.J., Moses, J.D., et al.: 1995, *Solar Phys.* **162**, 357. DOI.
- Dai, Y., Zong, W.G., Tang, Y.H.: 2002, *Chin. Astron. Astrophys.* **26**, 183. DOI.
- Forbes, T.G.: 2000, *J. Geophys. Res.* **105**, 23153. DOI.
- Gopalswamy, N., Lara, A., Yashiro, S., Howard, R.A.: 2003, *Astrophys. J.* **598**, 63. DOI.
- Gopalswamy, N., Nunes, S., Yashiro, S., Howard, R.A.: 2004, *Adv. Space Res.* **33**, 676. DOI.
- Howard, R.A., Brueckner, G., St. Cyr, O.C., Biesecker, K., Dere, K., Koomen, M.J., et al.: 1997, *Geophys. Monogr.* **99**, 17. DOI.
- Howard, R.A., Sheeley, N.R. Jr., Michels, D.J., Koomen, M.J.: 1985, *J. Geophys. Res.* **90**, 8173. DOI.
- Lin, J., Forbes, T.G., Isenberg, P.A., Démoulin, P.: 1998, *Astrophys. J.* **504**, 1006. DOI.
- Michalek, G.: 2009, *Astron. Astrophys.* **494**, 263. DOI.
- Michalek, G.: 2012, *Solar Phys.* **276**, 277. DOI.
- Ming, Qu., Frank, Y., Ju, J., Haimin, W.: 2006, *Solar Phys.* **237**, 419. DOI.
- Mikić, Z., Linker, J.A.: 1994, *Astrophys. J.* **430**, 898. DOI.
- St. Cyr, O.C., Plunkett, S.P., Michels, D.J., Paswaters, S.E., Koomen, M.J., et al.: 2000, *J. Geophys. Res.* **105**, 169. DOI.
- Wen, Y., Maia, D., Wang, J.: 2007, *Astrophys. J.* **657**, 1117. DOI.
- Yashiro, S., Gopalswamy, N., Michalek, G., Howard, R.A.: 2003, *Adv. Space Res.* **32**, 2631. DOI.
- Yashiro, S., Gopalswamy, N., Michalek, G., St. Cyr, O.C., Plunkett, S.P., Rich, N.B., Howard, R.A.: 2004, *J. Geophys. Res.* **109**, A07105. DOI.